

VeFA: Vector-Based Feature Space Adaptation for Mitigating Forgetting in Fine-Tuning

Peng Wang¹ Minghao Gu¹ Qiang Huang¹

Abstract

Catastrophic forgetting is a well-documented challenge in model fine-tuning, particularly under small-data downstream regimes. Existing parameter-efficient fine-tuning methods operate primarily in weight space, which can cause overspecialization of the model to the limited observations of the downstream data. Recent work reveals that one mechanism underlying such forgetting is the introduction of intruder dimensions into the representation space during fine-tuning. To mitigate overwriting of pre-trained knowledge and enhance robustness, we propose Vector-based Feature Space Adaptation (VeFA), a new fine-tuning scheme that operates directly in feature space and avoids generating intruder dimensions. VeFA applies element-wise transformation to individual feature channels, ensuring that the effective fine-tuned weights will remain in the column space of the pre-trained weight matrix. We evaluate both standard fine-tuning performance (effectiveness) and the robustness of VeFA against LoRA on multiple tasks, including image classification, NLU, and NLG benchmarks. Across these tasks, VeFA achieves comparable fine-tuning performance while consistently showing less degree of forgetting.

1. Introduction

Pre-trained models on large-scale datasets have demonstrated strong generalization and transferable representations across a wide range of domains and tasks (Bommasani et al., 2021). However, due to distributional differences between the pre-training and downstream data, it is often necessary to fine-tune the pre-trained model. For example, a vision-language model such as CLIP (Radford et al.,

2021), pre-trained on web-scale image-text pairs, can be fine-tuned on Oxford-IIIT Pets for improved species recognition performance. Similarly, a language model such as GPT-2 (Radford et al., 2019), pre-trained on broad web text, can be fine-tuned on WebNLG (Gardent et al., 2017) for data-to-text generation. This pre-training-to-fine-tuning paradigm enables efficient knowledge transfer and is especially beneficial when downstream labels are scarce.

Fine-tuning is typically achieved by adjusting the pre-trained model in the weight space to better align with the distribution and characteristics of the downstream data (Devlin et al., 2019). Traditional methods include full fine-tuning and linear probing (Kumar et al., 2022). Full fine-tuning updates all the parameters of the pre-trained model using the downstream task data. Linear probing updates only the final linear layer of the frozen pre-trained model. To balance adaptation capability and efficiency, parameter-efficient fine-tuning (PEFT) methods have received increasing attention in recent years (Zaken et al., 2021; Houlsby et al., 2019; Hu et al., 2022). Among PEFT methods, LoRA (Hu et al., 2022) injects low-rank update matrices into frozen weights and achieves strong downstream adaptation. These PEFT approaches exceed the performance of linear probing while avoiding the computational and overfitting costs of full fine-tuning.

However, current fine-tuning methods primarily adapt the pre-trained model in the weight space and allow the learned representations to exit the column space induced by the pre-trained weight matrix. Intruder dimensions (Shuttleworth et al., 2024) can potentially be introduced during fine-tuning, adding new directions that are not present in the original pre-trained column space. Although this subspace escape increases expressivity and enables a tighter fit to the downstream data, it risks overwriting the general representations acquired during pre-training. As a result, this can lead to overfitting and catastrophic forgetting, particularly when downstream data are limited—a phenomenon commonly referred to as catastrophic forgetting (French, 1999; Kirkpatrick et al., 2017; Kemker et al., 2018; Serra et al., 2018). *The goal of this work is to constrain adaptation under the small-data downstream regime so that the model can exploit the additional expressivity of fine-tuning, while explicitly*

¹Department of Industrial and System Engineering, University of Southern California, Los Angeles, United States. Correspondence to: Qiang Huang <qianghua@usc.edu>, Peng Wang <pwang341@usc.edu>.

mitigating overfitting to the limited downstream samples and preventing forgetting of the broadly generalizable representations acquired during pre-training.

Weight-space fine-tuning methods typically assume that the input–output mapping learned during pre-training is insufficiently aligned with the downstream tasks. Consequently, they replace the pre-trained weights \mathbf{W}_0 with adapted weights \mathbf{W}_{ft} to achieve effective adaptation. However, the discrepancy between the pre-training dataset and the downstream dataset is often unknown or unmeasurable. Fine-tuning the model in its weight space using *limited downstream data* inevitably modifies partial model parameters, and therefore risks the loss of knowledge learned during the pre-training stage (forgetting). *Essentially, the fundamental question is how to represent and integrate the unobservable downstream data discrepancy into the pre-trained model.*

Instead of modifying weights in the weight space, we propose to fine-tune models in the feature space. The key insight is to constrain the adaptation at each layer so that the fine-tuned model always remains within the column space of the pre-trained \mathbf{W}_0 . This guarantees that downstream updates cannot drift away from the representational subspace established during large-scale pre-training, thereby better preserving the broad knowledge already encoded. Although such feature-space adaptation nominally reduces the expressive power compared to unconstrained weight-space adaptation, the over-parameterization of modern neural networks ensures that there is still ample capacity to fit downstream tasks (Kirkpatrick et al., 2017), enabling fine-tuned models to achieve comparable performance while exhibiting consistently stronger robustness. This design is further motivated by the fact that pre-training typically involves data that are orders of magnitude larger and more diverse than any downstream dataset, providing the pre-trained model with strong generalization and even zero-shot capability. Fine-tuning should therefore preserve and leverage the structure embedded in \mathbf{W}_0 rather than overwrite it, thereby ensuring stability while still accommodating downstream distributional shifts.

The feasibility of feature-space adaptation is grounded in the idea of effect equivalence modeling (EEM) of lurking variables (Sabbaghi & Huang, 2018): given observed inputs and outputs, EEM compensates the influence of unobservable downstream factors by mapping their effect onto the observed features within the column space of the pre-trained weights. The unobservable factors that cause domain discrepancy can be more formally described as lurking variables in statistics (Box, 1966; Joiner, 1981). A lurking variable is defined as a variable that has an important effect but is not included among the predictor variables under consideration. It may be omitted from the analysis because its

existence is unknown, its influence is assumed to be negligible, or relevant data are unavailable (Hunter & Crowley, 1979). As illustrated in Fig. 1, lurking variables \mathbf{U} can alter the probability distributions of both input \mathbf{X} and response \mathbf{y} in the observed data, thus affecting the observed association between them. This leads to a perceived inconsistency between the downstream data and the pre-trained data. By identifying the equivalent amount Δ of lurking variable effects through input transformation, the pre-trained model can be applied more effectively to the downstream domain without modifying its parameters.

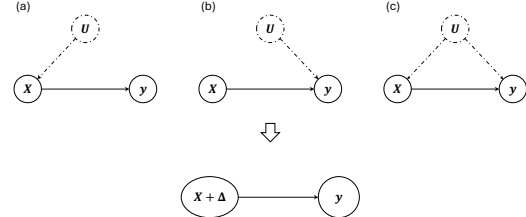


Figure 1. Three types of lurking variable impacts: (a) lurking variables \mathbf{U} only alter the distributions of input \mathbf{X} , (b) only alter output \mathbf{y} , or (c) alter both, all of which can be captured by the equivalent transformation.

Lurking variables are ubiquitous across application domains. In computer vision, style, texture, or lighting conditions can be viewed as lurking variables, systematically altering observed features while remaining unobserved and unlabeled during training (Mai et al., 2024). In natural language processing, language type or domain (e.g., news versus reports) influences syntactic and lexical patterns, yet is often ignored in modeling (Brown et al., 2020). More generally, distributional discrepancies between pre-training datasets (e.g., ImageNet, Wikipedia) and downstream benchmarks (e.g., Oxford Pets, CoLA) can be viewed as arising from lurking variables that affect the input–output relationship in downstream domains or tasks. In manufacturing applications, unobservable process changes such as machine calibration have been effectively modeled as lurking variables in 3D printing quality control (Huang et al., 2015; Sabbaghi & Huang, 2018). In causal inference, unmeasured confounding remains a classic example of lurking variables, which has been extensively studied in synthetic control (Abadie & Gardeazabal, 2003).

The remainder of this paper is organized as follows. In Section 2, we formally review the notion of intruder dimensions, their link to forgetting, and the EEM framework for lurking variables, which together provide the foundation of our study. In Section 3, we show how EEM can be utilized to design a new feature-space fine-tuning strategy. In Section 4, we present a theoretical analysis that introduces a new forgetting measure for pre-trained models based on intruder dimensions and explains why our fine-tuned model can explicitly control forgetting. Section 5 reports empirical

evaluations, demonstrating the effectiveness of the proposed approach, and Section 6 concludes the paper and outlines directions for future work.

2. Preliminaries

2.1. Intruder Dimension

Shuttleworth et al. (2024) introduced the concept of *intruder dimension* and discussed its impact on LoRA forgetting. In that work, the “direction” change between the pre-trained and fine-tuned weights was quantified by cosine similarity between the leading left singular vectors of the pre-trained and fine-tuned weight matrices obtained from their SVD decompositions. Although this is intuitive, cosine similarity is in general not a suitable notion of direction for weight matrices, because it is not invariant under natural symmetries of neural networks (Navon et al., 2023; Theus et al., 2025). For example, permuting the hidden units (and hence permuting the rows/columns of a weight matrix) yields a permuted model that produces exactly the same outputs as the original pre-trained model for all pre-training inputs and is therefore functionally equivalent to it (see the detailed discussion in the appendix B.1). Nevertheless, such a permutation will typically change the cosine similarity between the corresponding singular vectors, so a drop in cosine similarity in this case cannot be interpreted as the model having “forgotten” any knowledge. By contrast, the definition we introduce below depends only on the *singular subspaces* of the pre-trained and fine-tuned weights, and is therefore *invariant under such permutation symmetries*.

Let $\mathbf{W}_0 = \mathbf{U}_0 \Sigma_0 \mathbf{V}_0^\top$ be the singular value decomposition of the pre-trained weight matrix. Although \mathbf{W}_0 is typically full rank in a mathematical sense, it is not full rank numerically because its tail singular values are very small (e.g. 1×10^{-5}) (see the detailed discussion in the appendix B.2). To make the spectral analysis meaningful, we define

$$r_0 = \inf \left\{ r \in \mathbb{Z} : \sum_{i=1}^r \sigma_{0,i}^2 \geq \alpha \|\mathbf{W}_0\|_F^2 \right\}, \quad (1)$$

and, throughout this paper, approximate \mathbf{W}_0 using only its leading r_0 singular components as $\mathbf{W}_0 \approx \mathbf{U}_0[:, 1:r_0] \Sigma_0[1:r_0, 1:r_0] \mathbf{V}_0[:, 1:r_0]^\top$. Let $\mathbf{W}_{\text{ft}} = \mathbf{U}_{\text{ft}} \Sigma_{\text{ft}} \mathbf{V}_{\text{ft}}^\top$ be the singular value decomposition of the fine-tuned weight matrix, and let r_{ft} denote the number of its nonzero singular values. We define $\mathcal{S}_0 = \text{span}(\mathbf{U}_0[:, 1:r_0])$, and let \mathcal{S}_{ft} be the subspace spanned by the left singular vectors of \mathbf{W}_{ft} corresponding to its nonzero singular values. A unit vector $\mathbf{u} \in \mathcal{S}_{\text{ft}}$ is an *intruder dimension* of \mathbf{W}_{ft} w.r.t. \mathbf{W}_0 if $\|P_{\mathcal{S}_0} \mathbf{u}\|_2^2 < \varepsilon$, where $P_{\mathcal{S}_0}$ is the orthogonal projector onto \mathcal{S}_0 . In this paper, we will establish a mathematical link between *intruder dimensions* and *catastrophic forgetting*, and propose a principled approach to mitigating the impact

of such *intruder dimensions*.

2.2. Effect Equivalence Modeling of Lurking Variables

In modeling a system’s responses $\mathbf{y} \in \mathbb{R}^k$, it is useful to distinguish two categories of influencing variables: (i) observable variables \mathbf{X} that are measured and available for analysis, and (ii) lurking variables \mathbf{U} that are unobserved, ignored, or lack corresponding data yet may introduce variability (Box, 1966; Hunter & Crowley, 1979). Standard assumptions typically treat \mathbf{X} as the sole explanatory factors and regard \mathbf{U} as fixed or negligible. Under these assumptions, the system is modeled as $\mathbf{y} = f(\mathbf{X}) + \epsilon$, where $f : \mathbb{R}^d \rightarrow \mathbb{R}^k$ denotes the response map and ϵ is a k -dimensional noise term ($\mathbb{E}[\epsilon] = \mathbf{0}$ and $\text{Cov}(\epsilon) = \Sigma$). However, when such assumptions are violated (more aligned with real-world scenarios such as the downstream data with unknown discrepancy with the pre-training data), the response should instead be modeled as

$$\mathbf{y} = g(\mathbf{X}, \mathbf{U}) + \epsilon \quad (2)$$

where lurking variables \mathbf{U} exert non-negligible influence. When the usual assumptions are met, Eq. 2 is degenerated into Eq. 3 and $f(\cdot)$ has a simpler form.

$$\mathbf{y} = g(\mathbf{X}, \mathbf{U} = \mathbf{0}) + \epsilon = f(\mathbf{X}) + \epsilon \quad (3)$$

However, when lurking variables are present, they pose a challenging question: how can one infer and account for their effects when direct observation is not accessible? The work in (Huang et al., 2015; Sabbaghi & Huang, 2018) developed the EEM approach to model the effects of lurking variables to improve 3D printing accuracy.

Definition 1 (EEM). Let $g : \mathbb{R}^d \times \mathbb{R}^m \rightarrow \mathbb{R}^k$ be a k -dimensional response function defined on observable variables \mathbf{X} and lurking variables \mathbf{U} . Assume $g \in C^1(\mathbb{R}^d \times \mathbb{R}^m)$ and that for each $i \in \{1, \dots, d\}$, the partial derivative $\frac{\partial g}{\partial x_i}(\mathbf{X}, \mathbf{0}) \in \mathbb{R}^k$ is non-zero. The total equivalent amount of lurking-variable effects Δ in terms of \mathbf{X} can then be estimated from the data.

$$g(\mathbf{X}, \mathbf{U}) = g(\mathbf{X} + \Delta, \mathbf{U} = \mathbf{0}) = f(\mathbf{X} + \Delta) \quad (4)$$

The justification follows from the mean value theorem applied to a first-order Taylor expansion. There is no explicit solution for Δ , but it can be estimated through statistical learning or neural networks using the observed variables \mathbf{X} as input.

Lurking variables can explain the source of discrepancy between the pre-training dataset and the downstream dataset: unobserved or missing features prevent the pre-trained model from being directly applied to the downstream domain or task. EEM therefore provides a solution to mitigate the influence of lurking variables and also *offers a perspective for performing fine-tuning in the feature space without changing model parameters*.

3. Methodology

3.1. Problem Setup

We evaluate the robustness/forgetting of fine-tuning methods using established criteria from the literature (Wortsman et al., 2022): fine-tuning on a single downstream dataset should not reduce accuracy on other downstream datasets compared to the zero-shot model. In this work, robustness is therefore interpreted as being inversely related to forgetting—methods that induce less forgetting are regarded as more robust.

Firstly, we present the general formulation for model fine-tuning. Let $f_{\mathbf{W}_0} : \mathcal{X} \rightarrow \mathcal{Y}$ be a pre-trained model with parameters \mathbf{W}_0 . Given a downstream dataset \mathcal{D}_{ft} , fine-tuning solves

$$\begin{aligned}\mathbf{W}_{\text{ft}} &= \arg \min_{\mathbf{W} \in \mathcal{A}} \mathcal{L}(\mathbf{W}; \mathcal{D}_{\text{ft}}), \\ \mathcal{L}(\mathbf{W}; \mathcal{D}_{\text{ft}}) &= \mathbb{E}_{(\mathbf{X}, \mathbf{y}) \sim \mathcal{D}_{\text{ft}}} [\ell(\mathbf{X}, \mathbf{y}; f_{\mathbf{W}})],\end{aligned}$$

where \mathcal{A} encodes the adaptation family (e.g., full fine-tuning and LoRA) and $\mathcal{L}(\mathbf{W}; \mathcal{D}_{\text{tr}})$ denotes the loss function of \mathbf{W} for fine-tuning dataset \mathcal{D}_{tr} .

In practice, the choice of loss function \mathcal{L} depends on the downstream task: cross-entropy for classification, mean squared error for regression, and token-level negative log-likelihood for natural language generation tasks.

For full fine-tuning, \mathbf{W} is initialized at the pre-trained parameters $\mathbf{W}_0 = \{\mathbf{W}_0^{(l)}\}_{l=1, \dots, L}$ (where L denotes the number of learnable layers in the pre-trained model), and update all components end to end. For LoRA, each layer weight $\mathbf{W}_0^{(\ell)} \in \mathbb{R}^{p \times q}$ is frozen and augmented with a low-rank update $\mathbf{B}^{(\ell)} \mathbf{A}^{(\ell)}$, where $\mathbf{A}^{(\ell)} \in \mathbb{R}^{r \times q}$ and $\mathbf{B}^{(\ell)} \in \mathbb{R}^{p \times r}$ with $r \ll \min(p, q)$. The fine-tuned weight is

$$\mathbf{W}_{\text{ft}}^{(\ell)} = \mathbf{W}_0^{(\ell)} + \mathbf{B}^{(\ell)} \mathbf{A}^{(\ell)} \quad (5)$$

and only the low-rank parameters $\mathbf{A}^{(\ell)}, \mathbf{B}^{(\ell)}$ are optimized.

Secondly, we consider cross-dataset robustness in the proposed fine-tuning formulation. Under this setup, we assess how fine-tuning on one downstream domain/task affects zero-shot generalization to a different domain/task under distribution shift. Concretely, suppose we fine-tune the pre-trained model $f_{\mathbf{W}_0}$ on a dataset $\mathcal{D}_{\text{ft}}^{(a)}$, obtaining the adapted parameters \mathbf{W}_{ft} . The resulting model $f_{\mathbf{W}_{\text{ft}}}$ is assessed not only on the in-domain/task test set $\mathcal{D}_{\text{te}}^{(a)}$, but also on out-of-domain/task test sets $\{\mathcal{D}_{\text{te}}^{(b)} : b \neq a\}$ corresponding to other downstream datasets. Robustness is measured by the relative change in task-specific metric \mathcal{M} (where larger values indicate better performance) compared to the zero-shot pre-trained model $f_{\mathbf{W}_0}$:

$$R^{(b)} = \mathcal{M}(f_{\mathbf{W}_{\text{ft}}}, \mathcal{D}_{\text{te}}^{(b)}) - \mathcal{M}(f_{\mathbf{W}_0}, \mathcal{D}_{\text{te}}^{(b)}). \quad (6)$$

A fine-tuned model $f_{\mathbf{W}_{\text{ft}}}$ is *robust* if $R^{(b)} \geq -\epsilon$ for all $b \neq a$.

3.2. Vector-based Feature Space Adaptation (VeFA)

Rather than blindly updating all parameters or indiscriminately altering the pre-trained model’s weight space, one should first understand how the downstream distribution differs from the pre-trained dataset. For example, in image classification, class semantics are largely stable across domains, while discrepancies typically arise from style, background, resolution, illumination, viewpoint, and other contextual factors. These factors act as lurking variables that confound the input while leaving intrinsic class semantics unchanged.

Inspired by the EEM view of lurking variables, we propose to perform fine-tuning directly in the feature space via Vector-based Feature Space Adaptation (VeFA). Concretely, we keep $\mathbf{W}_0^{(\ell)}$ frozen and introduce a diagonal feature-wise scaling matrix $\Lambda^{(\ell)}$, yielding the following model for the ℓ -th layer:

$$\begin{aligned}\mathbf{h}^{(\ell)} &= \mathbf{W}_0^{(\ell)} \left(\mathbf{h}^{(\ell-1)} + \boldsymbol{\lambda}^{(\ell)} \odot \mathbf{h}^{(\ell-1)} \right) \\ &= \mathbf{W}_0^{(\ell)} \left(\mathbf{I} + \boldsymbol{\Lambda}^{(\ell)} \right) \mathbf{h}^{(\ell-1)} = \mathbf{W}_{\text{ft}}^{(\ell)} \mathbf{h}^{(\ell-1)}\end{aligned}$$

where \mathbf{I} is the identity matrix and $\boldsymbol{\Lambda}^{(\ell)} = \text{diag}(\boldsymbol{\lambda}^{(\ell)})$ performs channel-wise scaling of the layer input. Essentially, compared to LoRA (Fig. 2a), the updating rule of VeFA (Fig. 2b) is:

$$\mathbf{W}_{\text{ft}}^{(\ell)} = \mathbf{W}_0^{(\ell)} + \mathbf{W}_0^{(\ell)} \boldsymbol{\Lambda}^{(\ell)} \quad (7)$$

The vector $\boldsymbol{\lambda}$ is initialized to zero.

Compared to LoRA, VeFA is substantially more parameter-efficient. To our knowledge, VeFA actually ranks among the most parameter-efficient LoRA-style variants, especially compared to approaches such as VeRA (Kopczko et al., 2023). In addition, all VeFA updates are constrained to the column space of the pre-trained weight matrix: $\text{Col}(\mathbf{W}_0 \boldsymbol{\Lambda}^{(\ell)}) \subseteq \text{Col}(\mathbf{W}_0)$. VeFA preserves the representation subspace of \mathbf{W}_0 and does not introduce any intruder dimensions, as illustrated in Fig. 2(c).

We restrict adaptation to channel-wise scaling of the hidden representation without cross-channel mixing for practical reasons. First, recent work on *sparsifying large neural networks* (e.g., sparse attention post-training for mechanistic interpretability (Draye et al., 2025) and weight-sparse transformers with interpretable circuits (Gao et al., 2025)) suggests that modern large-scale models are highly over-parameterized and contain substantial redundancy: many weights can be pruned or sparsified with little loss in performance. Second, downstream fine-tuning datasets are typically much smaller and semantically narrower than the pre-training datasets, implying that the effective function required for the downstream task is often considerably simpler than the original pre-trained model. Therefore, the information encoded in the pre-trained model is even more redundant.

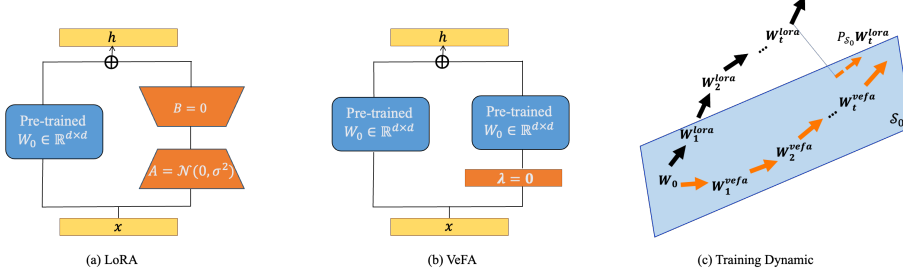


Figure 2. Schematic comparison of LoRA (a), VeFA (b) and their training dynamics (c). LoRA updates the weights matrix \mathbf{W} by training the low-rank matrices \mathbf{A} and \mathbf{B} , with intermediate rank r . VeFA keeps the pre-trained \mathbf{W}_0 frozen and performs adaptation at the element-wise feature level.

To compare weight-space and feature-space adaptation schemes, we first give a conceptual illustration. For weight-space adaptation, fine-tuning treats the neurons as fixed and updates the connection weights between them. Both hidden layers and the output layer acquire new trainable parameters. For feature-space adaptation, the original connection weights are frozen, and only lightweight, neuron-wise transformations are learned on top of the pre-trained features. This keeps the representational backbone intact, while still allowing task-specific adaptation through feature scaling.

To better understand their differences, we then give a simple one-dimensional example. Suppose that the pre-trained model is $y = 5x$, and the downstream dataset consists of $\{[0.2, 0.4], [0.6, 1.1], [1.1, 2.2], [1.6, 2.8]\}$. Using gradient descent, we estimate δ_1 in $y = (5 + \delta_1)x$ (weight-space adaptation) and δ_2 in $y = 5(x + \delta_2x)$ (feature-space adaptation). The final results are shown in the Fig. 3. In weight-space fine-tuning, the model adapts by directly updating the parameters, which shifts the regression line (purple dashed) away from the pre-trained function $f(x) = 5x$ in second sub-figure. In feature-space fine-tuning, the pre-trained model is kept frozen and adaptation is achieved by learning a lightweight transformation $\Delta(x)$ applied to the input features (orange dashed line in first sub-figure), resulting in the orange dashed regression line in second sub-figure.

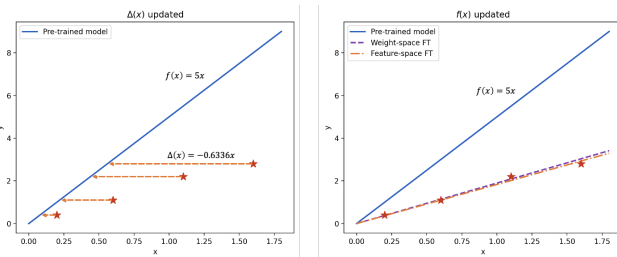


Figure 3. Comparison of weight-space fine-tuning and feature-space fine-tuning

It is worth noting that our method has a different focus from existing feature adaptation research. In prior work,

“features” refer to the outputs of a feature extractor, which are then modified to improve downstream transfer—such as CLIP adaptation (Gao et al., 2024), incremental learning (Ischen et al., 2020), or domain adaptation (Chen et al., 2019; Zheng et al., 2020). In contrast, we perform layer-wise feature adaptation to avoid introducing intruder dimensions.

4. Theoretical Analysis

In this section, we introduce a mathematical interpretation of how forgetting is related to *intruder dimensions*, and rigorously analyze why VeFA can effectively control forgetting based on the interpretation. We focus on a linear regression setting with mean-squared loss. The data distribution of the downstream task is generated by the underlying true model $\mathbf{y} = \mathbf{W}^* \mathbf{x} + \varepsilon$ with i.i.d. noise ε . Let \mathbf{W}_0 and $\mathbf{W}_{\text{ft}} = \mathbf{W}_0 + \Delta$ denote the pre-trained and fine-tuned weight matrices, respectively. The rank of \mathbf{W}_0 is r_0 , as defined in Eq. 1.

Under this setting, the increase in the expected loss over the data distribution (expected risk) is studied:

$$\mathcal{L}(\mathbf{W}_{\text{ft}} | \mathbf{x}, \mathbf{y}) - \mathcal{L}(\mathbf{W}_0 | \mathbf{x}, \mathbf{y}) = \text{Tr}(\Delta \Sigma_{\mathbf{x}} \Delta^T) \quad (8)$$

where \mathbf{x} and \mathbf{y} follow the pre-training data distribution, and $\Sigma_{\mathbf{x}} = \mathbb{E}(\mathbf{x} \mathbf{x}^T)$ denotes the empirical covariance matrix of the pre-training data.

This increase in the expected loss quantifies the degradation in model generalization after fine-tuning, capturing effects related to catastrophic forgetting and reduced robustness. A straightforward approach implied by Eq. 8 is to regulate the norm of Δ (that is, to impose a constraint on the magnitude of the update), which is exactly the key strategy adopted by many works on mitigating catastrophic forgetting (Kirkpatrick et al., 2017) and on robust fine-tuning (Gouk et al., 2020; Tian et al., 2023).

In this paper, we carry out an in-depth analysis of the increased expected loss by decomposing Eq. 8 and linking it to the intruder dimension. Recall that \mathcal{S}_0 denotes the column space of \mathbf{W}_0 , let $P_{\mathcal{S}_0}$ and $P_{\mathcal{S}_0}^\perp$ be the or-

thogonal projections onto \mathcal{S}_0 and its orthogonal complement. Then the update Δ admits the decomposition as $\Delta = P_{\mathcal{S}_0}\Delta + P_{\mathcal{S}_0}^\perp\Delta = \Delta_{\parallel} + \Delta_{\perp}$. Then

$$\text{Tr}(\Delta\Sigma_x\Delta^\top) = \text{Tr}(\Delta_{\parallel}\Sigma_x\Delta_{\parallel}^\top) + \text{Tr}(\Delta_{\perp}\Sigma_x\Delta_{\perp}^\top). \quad (9)$$

The cross term is canceled as the result of cyclic property of trace and $P_{\mathcal{S}_0}P_{\mathcal{S}_0}^\perp = \mathbf{0}$. We can see that both terms in the decomposition (9) are non-negative, and the positive loss increase is expected since \mathbf{W}_0 is the best estimator for the pre-training data. To the best of our knowledge, Eq. 8 and 9 provide the first general formulation to quantify forgetting in terms of the increase in expected risk, independent of specific fine-tuning mechanism such as LoRA or its variants. This quantitative metric is not restricted to evaluating PEFT approaches; in principle, it can be used in a wide variety of forgetting-related scenarios, including continual learning.

The first loss term of in Eq. 9 corresponds to the effect of transformations within the column space of \mathbf{W}_0 , while the second term captures the forgetting or harmful effect introduced by intruder dimensions. For VeFA, the second loss term in Eq. 9 is zero, which means that VeFA does not suffer from the intruder-dimension-induced forgetting that arises in LoRA.

Eq. 9 also suggests that when intruder dimensions are introduced, this second loss term becomes strictly positive. To quantify the additional forgetting purely attributed to intruder directions, Proposition 4.1 below provides an explicit lower bound of the increased loss. The proof of Proposition 4.1 can be found in Appendix D.1.

Proposition 4.1. *If $P_{\mathcal{S}_0}^\perp\Delta \neq \mathbf{0}$, the increase in expected loss attributable to the intruder dimensions admits a lower bound:*

$$\begin{aligned} \text{Tr}(\Delta_{\perp}\Sigma_x\Delta_{\perp}^\top) &\geq \sigma_{\min}(\Sigma_x) \left(\sqrt{(1-\varepsilon)r_{\text{ft}}\sigma_{\text{ft},r_{\text{ft}}}^2} \right. \\ &\quad \left. - \sqrt{1-\alpha}\|\mathbf{W}_0\|_F \right)_+^2. \end{aligned}$$

For VeFA, we further prove that the first loss term in Eq. 9 has an upper bound, as specified by Proposition 4.2 (proof can be seen in Appendix D.2). Notably, the bound depends only on the maximum absolute entry of the diagonal vector λ , so enforcing $\|\lambda\|_\infty \leq \gamma$ yields a global bound on the total forgetting under VeFA. In the next section, we also show with experiments that, for most tasks, $\max_j |\lambda_j|$ of the fine-tuned matrices remains small even without any explicit constraint. For more challenging tasks, one can additionally impose an explicit upper bound on $\max_j |\lambda_j|$, which directly controls the overall forgetting (seen in Appendix E.1).

Proposition 4.2. *Assume that Σ_x and $\|\mathbf{W}_0\|_F$ are bounded. For VeFA, the in-subspace loss term satisfies*

$$\text{Tr}\left(P_{\mathcal{S}_0}\Delta\Sigma_x\Delta^\top P_{\mathcal{S}_0}^T\right) \leq \|\Sigma_x\|_2\|\mathbf{W}_0\|_F^2\left(\max_j |\lambda_j|\right)^2.$$

In summary, VeFA introduces no intruder dimensions and therefore avoids the associated intruder-induced forgetting.

Within the original main column space of \mathbf{W}_0 , the transformation loss is tightly bounded and controlled by the small feature-wise scaling factors λ , so the overall forgetting under VeFA remains bounded. Consequently, VeFA exhibits substantially reduced catastrophic forgetting and correspondingly strong robustness.

5. Experiment

5.1. Experiment setup

Pre-trained models and downstream tasks. To demonstrate the effectiveness of VeFA, we fine-tune three different pre-trained model on their corresponding downstream datasets. Our goals are twofold: (i) to show that VeFA achieves comparable downstream performance to LoRA while using substantially fewer trainable parameters, and (ii) to examine, through multiple cross-task evaluations, whether VeFA attains better performance than LoRA in terms of reduced forgetting and thus improved robustness.

1. Image Classification (CLIP across seven datasets (Radford et al., 2021; Zanella & Ben Ayed, 2024)). We fine-tune CLIP (ViT-B/16 backbone) on seven image classification datasets. In each case, the model is fine-tuned on one dataset and then evaluated on the others. By comparing fine-tuned performance with CLIP’s zero-shot baseline, we assess the cross-dataset robustness of different fine-tuning strategies.

2. Natural Language Understanding (RoBERTa on GLUE(Liu et al., 2019; Wang et al., 2018)). We evaluate RoBERTa on the GLUE benchmark. Since GLUE requires task-specific classification heads, we do not merge all tasks into a single shared head for robustness evaluation. Instead, for each target task, we keep its own fine-tuned classification head, federated-average (McMahan et al., 2017) the VeFA adapters trained on the other GLUE tasks into one shared backbone, and then evaluate this merged backbone together with the target task’s head on that task, without any further fine-tuning. The resulting performance, compared against the zero-shot RoBERTa baseline on the same task, serves as our robustness and forgetting measure for NLU.

3. Natural Language Generation (GPT-2 on E2E (Radford et al., 2019; Novikova et al., 2017)). We fine-tune GPT-2 on the E2E NLG benchmark, which provides a relatively data-rich downstream setting compared to typical few-shot settings. Here the goal is to assess effectiveness: we test whether VeFA’s constrained, channel-wise adaptation can still match LoRA’s performance when more downstream data are available.

5.2. Fine-tuning CLIP for Image Classification

We follow the setting of previous work (Zhou et al., 2022; Zanella & Ben Ayed, 2024). We evaluate on seven datasets

spanning diverse visual domains—satellite imagery (EuroSAT (Helber et al., 2019)), food (Food101 (Bossard et al., 2014)), pet breeds (OxfordPets (Parkhi et al., 2012)), flowers (Flower102 (Nilsback & Zisserman, 2008)), generic objects (Caltech101 (Fei-Fei et al., 2004)), textures (DTD (Cimpoi et al., 2014)), and human actions (UCF101 (Soomro et al., 2012)). Together, these datasets provide a comprehensive benchmark for visual classification.

We compare VeFA, against LoRA (rank $r = 2$) in terms of few-shot learning performance and cross-dataset robustness. In few-shot learning, a “shot” refers to the number of labeled training examples provided per class. Few-shot learning closely matches the setting studied in this paper, where downstream data are much smaller in scale than the pre-training datasets and the goal is to mitigate overfitting and forgetting during fine-tuning. We conduct experiments under 1-shot, 4-shot, and 16-shot learning settings. The results are presented in Tab. 1. For the 1-shot and 4-shot settings, we report only effectiveness, whereas for the 16-shot setting, we report both effectiveness and robustness (see the last two rows of Tab. 1). With only 25% of LoRA’s trainable parameters, VeFA achieves higher average performance in the 1-shot, 4-shot, and 16-shot settings, and consistently shows superior robustness across all seven datasets. These results highlight VeFA’s advantage in low-data settings, enabling effective knowledge transfer while better preserving pre-trained representations.

5.3. Natural Language Understanding

We evaluate on the General Language Understanding Evaluation (GLUE) benchmark (Wang et al., 2018) using RoBERTa-base and RoBERTa-large (Liu et al., 2019). We compare VeFA against LoRA. Our experiment broadly follows the setting in LoRA (Hu et al., 2022): we adapt the query and value projection matrices in each self-attention block and fully train the task-specific classification head. Unlike (Hu et al., 2022), which employs an auxiliary hyperparameter α to rescale gradients in adapted layers, we use separate learning rates for (i) the classification head and (ii) the adapted layers. Learning rates and training epochs are chosen via hyperparameter tuning; full settings appear in Appendix C. We use batch size 64 for RoBERTa-base and 32 for RoBERTa-large respectively.

In line with Hu et al. (2022), we report the number of trainable parameters in the backbone layers, explicitly excluding the task-specific classification head, which is always trained in the standard way. For each setting we run five trials with different random seeds, take the best epoch in each trial, and report the median over these five results. We also reproduce the original LoRA results under the same experimental setup as in Hu et al. (2022) and observe that our SVD-initialized models achieve nearly identical performance, indicating that

the SVD approximation does not affect fine-tuning. To evaluate cross-task robustness, we use only the checkpoint with the median validation performance among the 5 runs. For a given GLUE task, we keep its own classification head fixed and federated-average the adapters trained on the other GLUE tasks into a single shared backbone. The robustness metric is then defined as the difference in the task-specific score between this merged-backbone model and the baseline model that uses the original GPT-2 backbone with the same classification head.

The experimental results of effectiveness are presented in Tab. 2. VeFA achieves performance comparable to LoRA across both models, while requiring an order of magnitude fewer parameters. The cross-task robustness results are shown in Table 3, where VeFA achieves stronger cross-task robustness than LoRA.

5.4. Natural Language Generation

We evaluate on the E2E benchmark (Novikova et al., 2017), following the experimental protocol used for LoRA (Hu et al., 2022), and fine-tune GPT-2 Medium and Large (Radford et al., 2019). In this setting, the downstream task is more complex, and the dataset is substantially larger than in our visual classification and NLU experiments. Our goal is to test whether VeFA still retains sufficient expressive power under such a challenging regime. For a fair comparison, we run LoRA and VeFA within the same experimental platform. For LoRA, we use the official hyperparameters from (Hu et al., 2022), while a complete list of the hyperparameters used for VeFA is provided in Appendix C. Moreover, We bound VeFA’s scaling vector by clipping each entry of λ to $[-2, 2]$, so that $\|\lambda\|_\infty \leq 2$ throughout training, as shown in Appendix E.1.

The E2E benchmark contains a single task: given a meaning representation, generate natural-language descriptions. We evaluate with five metrics—BLEU, NIST, MET, ROUGE-L, and CIDEr—to comprehensively assess generation quality. We report the results from the final epoch. As shown in Tab. 4, VeFA achieves performance comparable to LoRA on both GPT-2 Medium and GPT-2 Large, while using substantially fewer trainable parameters.

6. Conclusion

To mitigate forgetting during fine-tuning, this work proposes a feature-space fine-tuning framework grounded in effect-equivalence modeling, as an alternative to conventional weight-space update strategies. Through theoretical analysis, we explicitly quantify a forgetting measure and relate it to intruder dimensions. We show that VeFA introduces no intruder dimensions and therefore avoids the loss induced by them. We further derive a global bound on the

Table 1. Performance comparison between LoRA and VeFA across different datasets under zero-shot, 1-shot, 4-shot, 16-shot fine-tuning, and robustness. The visual backbone is ViT-B/16. Better results are in **bold**.

| Shots | Type | Caltech101 | Food101 | Oxford Pets | Oxford Flowers | EuroSAT | DTD | UCF101 |
|-----------|------|-------------|-------------|-------------|----------------|-------------|-------------|-------------|
| 0 | CLIP | 93.2 | 85.2 | 88.2 | 67.3 | 42.3 | 44.3 | 65.0 |
| 1 | LoRA | 94.0 | 82.3 | 91.8 | 79.4 | 71.8 | 53.0 | 75.4 |
| | VeFA | 94.1 | 86.3 | 93.3 | 84.3 | 73.3 | 55.0 | 74.2 |
| 4 | LoRA | 95.2 | 81.6 | 90.8 | 93.8 | 87.5 | 62.2 | 78.5 |
| | VeFA | 95.6 | 86.0 | 93.4 | 93.0 | 87.1 | 65.7 | 80.2 |
| 16 | LoRA | 96.3 | 84.0 | 91.3 | 98.2 | 90.2 | 71.8 | 86.2 |
| | VeFA | 96.4 | 87.8 | 94.4 | 97.5 | 91.3 | 72.5 | 86.4 |
| \bar{R} | LoRA | -2.4 | -3.8 | -2.8 | -4.4 | -14.1 | -3.0 | -1.1 |
| | VeFA | +0.2 | -0.6 | -0.4 | +0.4 | -2.3 | +2.0 | +0.3 |

Table 2. Performance on GLUE with different fine-tuning methods. We report Matthews correlation for CoLA, Pearson correlation for STS-B, and accuracy for all other tasks; higher is better. Results for all methods except VeFA and LoRA are taken from prior work (Hu et al., 2022; Kopiczko et al., 2023).

| | Type | # Params | SST-2 | MRPC | CoLA | QNLI | RTE | STS-B | AVG |
|-------|--------|---------------|----------------|----------------|----------------|----------------|----------------|----------------|------|
| Base | FT | 125M | 94.8 | 90.2 | 63.6 | 92.8 | 78.7 | 91.2 | 85.2 |
| | BitFit | 0.1M | 93.7 | 92.7 | 62.0 | 91.8 | 81.5 | 90.8 | 85.4 |
| | Adpt | 0.3M | 94.2 \pm 0.1 | 88.5 \pm 1.1 | 60.8 \pm 0.4 | 93.1 \pm 0.1 | 71.5 \pm 2.7 | 89.7 \pm 0.3 | 83.0 |
| | LoRA | 0.3M | 94.7 \pm 0.2 | 90.1 \pm 0.9 | 64.7 \pm 1.6 | 92.6 \pm 0.2 | 86.6 \pm 0.9 | 91.4 \pm 0.1 | 86.7 |
| | VeRA | 0.043M | 94.6 \pm 0.1 | 89.5 \pm 0.5 | 65.6 \pm 0.8 | 91.8 \pm 0.2 | 78.7 \pm 0.7 | 90.7 \pm 0.2 | 85.2 |
| | VeFA | 0.018M | 94.1 \pm 0.1 | 88.5 \pm 0.7 | 63.3 \pm 1.0 | 91.7 \pm 0.2 | 83.0 \pm 0.4 | 90.7 \pm 0.1 | 85.2 |
| Large | LoRA | 0.8M | 96.2 \pm 0.2 | 89.7 \pm 1.1 | 66.0 \pm 2.0 | 94.8 \pm 0.3 | 90.2 \pm 0.6 | 92.4 \pm 0.3 | 88.2 |
| | VeRA | 0.061M | 96.1 \pm 0.1 | 90.9 \pm 0.7 | 68.0 \pm 0.8 | 94.4 \pm 0.2 | 85.9 \pm 0.7 | 91.7 \pm 0.8 | 87.8 |
| | VeFA | 0.049M | 95.8 \pm 0.2 | 90.4 \pm 0.8 | 68.0 \pm 1.2 | 94.1 \pm 0.3 | 87.0 \pm 0.4 | 91.2 \pm 0.4 | 87.8 |

Table 3. Cross-task robustness on GLUE via federated merging of medium-checkpoint adapters.

| | Type | SST-2 | MRPC | CoLA | QNLI | RTE | STS-B | AVG |
|-------|------|-------|------|------|------|------|-------|--------------|
| Base | LoRA | 15.9 | 0.0 | -2.0 | 3.3 | -0.1 | 15.8 | 5.48 |
| | VeFA | 4.7 | 0.0 | -4.0 | 5.7 | 1.1 | 43.7 | 8.53 |
| Large | LoRA | -2.0 | 0.0 | 0.0 | 0.1 | -1.1 | 34.0 | 5.17 |
| | VeFA | 11.0 | 6.8 | 14.1 | 8.7 | 11.2 | 59.0 | 18.47 |

Table 4. Performance comparison of LoRA and VeFA on GPT-2 Medium and GPT-2 Large using standard NLG evaluation metrics.

| | Type | # Params | BLEU | NIST | MET | ROUGE-L | CIDEr |
|--------|------|----------|-------|--------|-------|---------|--------|
| Medium | LoRA | 0.35M | 67.04 | 8.5753 | 45.92 | 68.74 | 2.3507 |
| | VeFA | 0.073M | 66.35 | 8.5628 | 44.79 | 66.93 | 2.2274 |
| Large | LoRA | 0.77M | 67.38 | 8.6293 | 45.98 | 68.82 | 2.3320 |
| | VeFA | 0.14M | 67.38 | 8.5889 | 46.11 | 68.86 | 2.3684 |

total forgetting under VeFA and rigorously show that it can be explicitly controlled, demonstrating VeFA’s robustness.

Our empirical results on vision and language tasks show that VeFA can match or even outperform weight-space fine-tuning approaches such as LoRA while using far fewer trainable parameters. VeFA also demonstrates stronger robustness across datasets. Overall, these results highlight

VeFA as an efficient alternative for achieving robustness and strong generalization.

Future research could explore alternative projected-gradient schemes that explicitly constrain the update Δ to the column space of W_0 while further reducing in-subspace loss. It could also investigate sparsity-inducing constraints on the scaling vector Λ , connecting VeFA to sparse and mechanistic interpretability.

Impact Statement

This work proposes VeFA, a feature-space fine-tuning method that improves robustness while substantially reducing the number of trainable parameters compared to common weight-space adaptation methods. By restricting adaptation to the column space of W_0 and avoiding intruder dimensions, VeFA can be particularly useful in low-data settings, where limited flexibility can improve reliability during deployment. We do not anticipate additional societal impacts beyond those commonly associated with improving the efficiency and robustness of model adaptation.

References

Abadie, A. and Gardeazabal, J. The economic costs of conflict: A case study of the basque country. *American economic review*, 93(1):113–132, 2003.

Bommasani, R., Hudson, D. A., Adeli, E., Altman, R., Arora, S., von Arx, S., Bernstein, M. S., Bohg, J., Bosse-lut, A., Brunskill, E., et al. On the opportunities and risks of foundation models. *arXiv preprint arXiv:2108.07258*, 2021.

Bossard, L., Guillaumin, M., and Van Gool, L. Food-101—mining discriminative components with random forests. In *European conference on computer vision*, pp. 446–461. Springer, 2014.

Box, G. E. Use and abuse of regression. *Technometrics*, 8(4):625–629, 1966.

Brown, T., Mann, B., Ryder, N., Subbiah, M., Kaplan, J. D., Dhariwal, P., Neelakantan, A., Shyam, P., Sastry, G., Askell, A., et al. Language models are few-shot learners. *Advances in neural information processing systems*, 33:1877–1901, 2020.

Chen, C., Xie, W., Huang, W., Rong, Y., Ding, X., Huang, Y., Xu, T., and Huang, J. Progressive feature alignment for unsupervised domain adaptation. In *Proceedings of the IEEE/CVF conference on computer vision and pattern recognition*, pp. 627–636, 2019.

Cimpoi, M., Maji, S., Kokkinos, I., Mohamed, S., and Vedaldi, A. Describing textures in the wild. In *Proceedings of the IEEE conference on computer vision and pattern recognition*, pp. 3606–3613, 2014.

Devlin, J., Chang, M.-W., Lee, K., and Toutanova, K. Bert: Pre-training of deep bidirectional transformers for language understanding. In *Proceedings of the 2019 conference of the North American chapter of the association for computational linguistics: human language technologies, volume 1 (long and short papers)*, pp. 4171–4186, 2019.

Draye, F., Lei, A., Posner, I., and Schölkopf, B. Sparse attention post-training for mechanistic interpretability. *arXiv preprint arXiv:2512.05865*, 2025.

Fei-Fei, L., Fergus, R., and Perona, P. Learning generative visual models from few training examples: An incremental bayesian approach tested on 101 object categories. In *2004 conference on computer vision and pattern recognition workshop*, pp. 178–178. IEEE, 2004.

French, R. M. Catastrophic forgetting in connectionist networks. *Trends in cognitive sciences*, 3(4):128–135, 1999.

Ganin, Y., Ustinova, E., Ajakan, H., Germain, P., Larochelle, H., Laviolette, F., March, M., and Lempitsky, V. Domain-adversarial training of neural networks. *Journal of machine learning research*, 17(59):1–35, 2016.

Gao, L., Rajaram, A., Coxon, J., Govande, S. V., Baker, B., and Mossing, D. Weight-sparse transformers have interpretable circuits. *arXiv preprint arXiv:2511.13653*, 2025.

Gao, P., Geng, S., Zhang, R., Ma, T., Fang, R., Zhang, Y., Li, H., and Qiao, Y. Clip-adapter: Better vision-language models with feature adapters. *International Journal of Computer Vision*, 132(2):581–595, 2024.

Gardent, C., Shimorina, A., Narayan, S., and Perez-Beltrachini, L. The webnlg challenge: Generating text from rdf data. In *10th International Conference on Natural Language Generation*, pp. 124–133. ACL Anthology, 2017.

Gouk, H., Hospedales, T. M., and Pontil, M. Distance-based regularisation of deep networks for fine-tuning. *arXiv preprint arXiv:2002.08253*, 2020.

Han, S., Pool, J., Tran, J., and Dally, W. Learning both weights and connections for efficient neural network. *Advances in neural information processing systems*, 28, 2015.

Helber, P., Bischke, B., Dengel, A., and Borth, D. Eurosat: A novel dataset and deep learning benchmark for land use and land cover classification. *IEEE Journal of Selected Topics in Applied Earth Observations and Remote Sensing*, 12(7):2217–2226, 2019.

Houlsby, N., Giurgiu, A., Jastrzebski, S., Morrone, B., De Laroussilhe, Q., Gesmundo, A., Attariyan, M., and Gelly, S. Parameter-efficient transfer learning for nlp. In *International conference on machine learning*, pp. 2790–2799. PMLR, 2019.

Hu, E. J., Shen, Y., Wallis, P., Allen-Zhu, Z., Li, Y., Wang, S., Wang, L., Chen, W., et al. Lora: Low-rank adaptation of large language models. *ICLR*, 1(2):3, 2022.

Huang, Q., Zhang, J., Sabbaghi, A., and Dasgupta, T. Optimal offline compensation of shape shrinkage for three-dimensional printing processes. *Iie transactions*, 47(5):431–441, 2015.

Hunter, W. G. and Crowley, J. J. Hazardous substances, the environment and public health: a statistical overview. *Environmental health perspectives*, 32:241–254, 1979.

Iscen, A., Zhang, J., Lazebnik, S., and Schmid, C. Memory-efficient incremental learning through feature adaptation. In *European conference on computer vision*, pp. 699–715. Springer, 2020.

Joiner, B. L. Lurking variables: Some examples. *The American Statistician*, 35(4):227–233, 1981.

Karimi Mahabadi, R., Henderson, J., and Ruder, S. Compacter: Efficient low-rank hypercomplex adapter layers. *Advances in neural information processing systems*, 34: 1022–1035, 2021.

Kemker, R., McClure, M., Abitino, A., Hayes, T., and Kanan, C. Measuring catastrophic forgetting in neural networks. In *Proceedings of the AAAI conference on artificial intelligence*, volume 32, 2018.

Kirkpatrick, J., Pascanu, R., Rabinowitz, N., Veness, J., Desjardins, G., Rusu, A. A., Milan, K., Quan, J., Ramalho, T., Grabska-Barwinska, A., et al. Overcoming catastrophic forgetting in neural networks. *Proceedings of the national academy of sciences*, 114(13):3521–3526, 2017.

Kopczko, D. J., Blankevoort, T., and Asano, Y. M. Vera: Vector-based random matrix adaptation. *arXiv preprint arXiv:2310.11454*, 2023.

Kumar, A., Raghunathan, A., Jones, R., Ma, T., and Liang, P. Fine-tuning can distort pretrained features and underperform out-of-distribution. *arXiv preprint arXiv:2202.10054*, 2022.

Lagunas, F., Charlaix, E., Sanh, V., and Rush, A. M. Block pruning for faster transformers. *arXiv preprint arXiv:2109.04838*, 2021.

Lee, C., Cho, K., and Kang, W. Mixout: Effective regularization to finetune large-scale pretrained language models. In *International Conference on Learning Representations*.

Lee, J., Park, S., Mo, S., Ahn, S., and Shin, J. Layer-adaptive sparsity for the magnitude-based pruning. *arXiv preprint arXiv:2010.07611*, 2020.

Liang, J., Hu, D., and Feng, J. Do we really need to access the source data? source hypothesis transfer for unsupervised domain adaptation. In *International conference on machine learning*, pp. 6028–6039. PMLR, 2020.

Liu, Y., Ott, M., Goyal, N., Du, J., Joshi, M., Chen, D., Levy, O., Lewis, M., Zettlemoyer, L., and Stoyanov, V. Roberta: A robustly optimized bert pretraining approach. *arXiv preprint arXiv:1907.11692*, 2019.

Mai, Z., Chowdhury, A., Zhang, P., Tu, C.-H., Chen, H.-Y., Pahuja, V., Berger-Wolf, T., Gao, S., Stewart, C., Su, Y., et al. Fine-tuning is fine, if calibrated. *Advances in Neural Information Processing Systems*, 37:136084–136119, 2024.

Mallya, A., Davis, D., and Lazebnik, S. Piggyback: Adapting a single network to multiple tasks by learning to mask weights. In *Proceedings of the European conference on computer vision (ECCV)*, pp. 67–82, 2018.

McMahan, B., Moore, E., Ramage, D., Hampson, S., and y Arcas, B. A. Communication-efficient learning of deep networks from decentralized data. In *Artificial intelligence and statistics*, pp. 1273–1282. PMLR, 2017.

Mostafa, H. and Wang, X. Parameter efficient training of deep convolutional neural networks by dynamic sparse reparameterization. In *International Conference on Machine Learning*, pp. 4646–4655. PMLR, 2019.

Motiian, S., Piccirilli, M., Adjero, D. A., and Doretto, G. Unified deep supervised domain adaptation and generalization. In *Proceedings of the IEEE international conference on computer vision*, pp. 5715–5725, 2017.

Navon, A., Shamsian, A., Achituv, I., Fetaya, E., Chechik, G., and Maron, H. Equivariant architectures for learning in deep weight spaces. In *International Conference on Machine Learning*, pp. 25790–25816. PMLR, 2023.

Nilsback, M.-E. and Zisserman, A. Automated flower classification over a large number of classes. In *2008 Sixth Indian conference on computer vision, graphics & image processing*, pp. 722–729. IEEE, 2008.

Novikova, J., Dušek, O., and Rieser, V. The e2e dataset: New challenges for end-to-end generation. *arXiv preprint arXiv:1706.09254*, 2017.

Panahi, A., Saeedi, S., and Arodz, T. Shapeshifter: a parameter-efficient transformer using factorized reshaped matrices. *Advances in Neural Information Processing Systems*, 34:1337–1350, 2021.

Parkhi, O. M., Vedaldi, A., Zisserman, A., and Jawahar, C. Cats and dogs. In *2012 IEEE conference on computer vision and pattern recognition*, pp. 3498–3505. IEEE, 2012.

Pfeiffer, J., Rücklé, A., Poth, C., Kamath, A., Vulić, I., Ruder, S., Cho, K., and Gurevych, I. Adapterhub: A framework for adapting transformers. *arXiv preprint arXiv:2007.07779*, 2020.

Radford, A., Wu, J., Child, R., Luan, D., Amodei, D., Sutskever, I., et al. Language models are unsupervised multitask learners. *OpenAI blog*, 1(8):9, 2019.

Radford, A., Kim, J. W., Hallacy, C., Ramesh, A., Goh, G., Agarwal, S., Sastry, G., Askell, A., Mishkin, P., Clark, J., et al. Learning transferable visual models from natural language supervision. In *International conference on machine learning*, pp. 8748–8763. PMLR, 2021.

Rücklé, A., Geigle, G., Glockner, M., Beck, T., Pfeiffer, J., Reimers, N., and Gurevych, I. Adapterdrop: On the efficiency of adapters in transformers. *arXiv preprint arXiv:2010.11918*, 2020.

Sabbaghi, A. and Huang, Q. Model transfer across additive manufacturing processes via mean effect equivalence of lurking variables. *The Annals of Applied Statistics*, 12(4): 2409–2429, 2018.

Sanh, V., Wolf, T., and Rush, A. Movement pruning: Adaptive sparsity by fine-tuning. *Advances in neural information processing systems*, 33:20378–20389, 2020.

Serra, J., Suris, D., Miron, M., and Karatzoglou, A. Overcoming catastrophic forgetting with hard attention to the task. In *International conference on machine learning*, pp. 4548–4557. PMLR, 2018.

Shuttleworth, R., Andreas, J., Torralba, A., and Sharma, P. Lora vs full fine-tuning: An illusion of equivalence. *arXiv preprint arXiv:2410.21228*, 2024.

Soomro, K., Zamir, A. R., and Shah, M. Ucf101: A dataset of 101 human actions classes from videos in the wild. *arXiv preprint arXiv:1212.0402*, 2012.

Theus, A., Cabodi, A., Anagnostidis, S., Orvieto, A., Singh, S. P., and Boeva, V. Generalized linear mode connectivity for transformers. *arXiv preprint arXiv:2506.22712*, 2025.

Tian, J., Liu, Y.-C., Smith, J. S., and Kira, Z. Fast trainable projection for robust fine-tuning. *Advances in Neural Information Processing Systems*, 36:11374–11393, 2023.

Wang, A., Singh, A., Michael, J., Hill, F., Levy, O., and Bowman, S. R. Glue: A multi-task benchmark and analysis platform for natural language understanding. *arXiv preprint arXiv:1804.07461*, 2018.

Wortsman, M., Ilharco, G., Kim, J. W., Li, M., Kornblith, S., Roelofs, R., Lopes, R. G., Hajishirzi, H., Farhadi, A., Namkoong, H., et al. Robust fine-tuning of zero-shot models. In *Proceedings of the IEEE/CVF conference on computer vision and pattern recognition*, pp. 7959–7971, 2022.

Xu, R., Luo, F., Zhang, Z., Tan, C., Chang, B., Huang, S., and Huang, F. Raise a child in large language model: Towards effective and generalizable fine-tuning. *arXiv preprint arXiv:2109.05687*, 2021.

Zaken, E. B., Ravfogel, S., and Goldberg, Y. Bitfit: Simple parameter-efficient fine-tuning for transformer-based masked language-models. *arXiv preprint arXiv:2106.10199*, 2021.

Zanella, M. and Ben Ayed, I. Low-rank few-shot adaptation of vision-language models. In *Proceedings of the IEEE/CVF Conference on Computer Vision and Pattern Recognition*, pp. 1593–1603, 2024.

Zheng, Y., Huang, D., Liu, S., and Wang, Y. Cross-domain object detection through coarse-to-fine feature adaptation. In *Proceedings of the IEEE/CVF conference on computer vision and pattern recognition*, pp. 13766–13775, 2020.

Zhou, K., Yang, J., Loy, C. C., and Liu, Z. Learning to prompt for vision-language models. *International Journal of Computer Vision*, 130(9):2337–2348, 2022.

Zhu, J.-Y., Park, T., Isola, P., and Efros, A. A. Unpaired image-to-image translation using cycle-consistent adversarial networks. In *Proceedings of the IEEE international conference on computer vision*, pp. 2223–2232, 2017.

A. Related Work

Parameter Efficient Fine Tuning (PEFT). PEFT aims to selectively fine-tune a small subset of parameters or incorporate lightweight trainable modules—a task that is inherently NP-hard. Existing PEFT approaches can be categorized into random approaches, rule-based approaches, and projection-based approaches based on how they choose which parameters to tune. **Randomized approaches**, such as the Random and Mixout models (Lee et al.), select parameters for fine-tuning without relying on task-specific data information. **Rule-based approaches** such as BitFit ((Zaken et al., 2021)), MagPruning ((Han et al., 2015; Lee et al., 2020; Lagunas et al., 2021)), Adapter ((Houlsby et al., 2019; Pfeiffer et al., 2020; Rücklé et al., 2020)), and LoRA ((Hu et al., 2022; Karimi Mahabadi et al., 2021; Panahi et al., 2021)) determine which parameters to fine-tune based on pre-defined heuristics. These methods incorporate prior knowledge to identify potentially important components in the model, thereby addressing some of the limitations of randomized approaches. However, the parameter selection process remains independent of the specific downstream data. Among rule-based PEFT methods, **LoRA** has become a de facto baseline due to its simplicity, hardware efficiency, and strong empirical performance across modalities. In our experiments, LoRA also serves as the primary baseline for comparison. **Projection-based approaches**, such as DiffPruning (Mallya et al., 2018; Sanh et al., 2020; Lagunas et al., 2021) and ChildPruning ((Xu et al., 2021; Mostafa & Wang, 2019)), aim to leverage task-specific data to guide the selection of tunable parameters in a pre-trained model. Our approach also falls under the category of PEFT; however, it differs fundamentally from prior PEFT methods in that we perform fine-tuning in the feature space rather than the weight space. Unlike weight-based methods, our fine-tuning does not alter the column space of W_0 , thereby preserving pre-training knowledge more effectively throughout adaptation. This design is particularly advantageous when fine-tuning large-scale models (e.g., the 175-billion-parameter GPT-3), where maintaining the integrity of pre-trained representations significantly improves robustness.

Domain Adaptation. Although our method explicitly models and compensates for domain discrepancy, it fundamentally differs from existing domain adaptation (DA) approaches (Zhu et al., 2017; Ganin et al., 2016; Liang et al., 2020; Motiian et al., 2017). DA methods generally rely on joint access to source and target data and seek to learn a domain-invariant representation by optimizing the feature extractor accordingly. In contrast, our problem setting assumes that source domain data is unavailable and needs to revise the pre-trained model to adapt to the downstream data. We perform feature-space transformation at the layer level, but the focus ultimately remains on parameter adaptation. Moreover, the domain discrepancy in our problem setting is substantially greater than that typically encountered in standard domain adaptation tasks. These distinctions position our work closer to fine-tuning methodologies rather than DA frameworks.

B. Neural Parameter Geometry

B.1. Cosine Similarity under Neural Parameter Symmetries

Neural networks exhibit rich *parameter symmetries*, meaning that different parameter values can define exactly the same function (Navon et al., 2023; Theus et al., 2025). Two examples that are particularly relevant for our analysis are permutation invariance and $GL(r)$ -invariance. For a two-layer MLP $f_{W_1, W_2}(x) = W_2\sigma(W_1x)$ and any permutation matrix P , the transformed parameters $W'_1 = PW_1$ and $W'_2 = W_2P^\top$ satisfy

$$f_{W'_1, W'_2}(x) = W_2P^\top\sigma(PW_1x) = f_{W_1, W_2}(x),$$

so permuting hidden units leaves the network function unchanged. Likewise, in modules that use low-rank matrix products—such as LoRA updates or the Q, K, V, W^O projections in attention—a rank- r factorization UV^\top is invariant under the action of any invertible matrix $R \in GL(r)$:

$$UV^\top = (UR)(VR^{-\top})^\top.$$

This $GL(r)$ -invariance reflects a “gauge freedom” in the choice of basis for the r -dimensional latent space: different pairs (U, V) related by such transformations represent the same linear map.

As a concrete illustration of permutation invariance, consider a two-layer network (with any pointwise activation σ) $h = \sigma(W_1x)$, $y = W_2h$, with

$$W_1 = \begin{pmatrix} 1 & 2 \\ 3 & 4 \end{pmatrix}, \quad W_2 = \begin{pmatrix} 5 & 6 \end{pmatrix}, \quad P = \begin{pmatrix} 0 & 1 \\ 1 & 0 \end{pmatrix}.$$

Define the permuted weights

$$W'_1 = PW_1 = \begin{pmatrix} 3 & 4 \\ 1 & 2 \end{pmatrix}, \quad W'_2 = W_2 P^\top = \begin{pmatrix} 6 & 5 \end{pmatrix}.$$

For any input $x = (x_1, x_2)^\top$ we obtain

$$h = W_1 x = \begin{pmatrix} x_1 + 2x_2 \\ 3x_1 + 4x_2 \end{pmatrix}, \quad h' = W'_1 x = \begin{pmatrix} 3x_1 + 4x_2 \\ x_1 + 2x_2 \end{pmatrix}.$$

The outputs of the original and permuted networks are

$$y = W_2 h = 5(x_1 + 2x_2) + 6(3x_1 + 4x_2), \quad y' = W'_2 h' = 6(3x_1 + 4x_2) + 5(x_1 + 2x_2),$$

$y' = y$ for all x . Thus, the parameter pairs (W_1, W_2) and (W'_1, W'_2) are functionally equivalent, even though their weight matrices differ and, in particular, the maximum absolute cosine similarity between any pair of their left singular vectors is only about 0.74. This example also shows that cosine similarity should not be used to define intruder dimensions associated with **forgetting**.

B.2. Rank analysis of the pre-trained weight matrix

Although in pre-trained models the weight matrices are mathematically full rank, their singular value spectra are concentrated. Most of the representational power of a pre-trained layer is carried by a low-dimensional principal subspace, while the remaining directions contribute only negligible energy. As illustrated in Fig. 4, for CLIP ViT-B/16, RoBERTa-base, and GPT-2 Medium, more than 99% of the spectral energy is already captured by roughly the top two-thirds of singular directions, with the remaining singular values quickly collapsing towards numerical noise. In our definition of intruder dimensions, we therefore restrict attention to this high-energy subspace: directions in the tiny-energy tail are poorly conditioned, highly sensitive to symmetries and optimization noise, and are unlikely to encode stable, semantically meaningful information that could be “forgotten.”

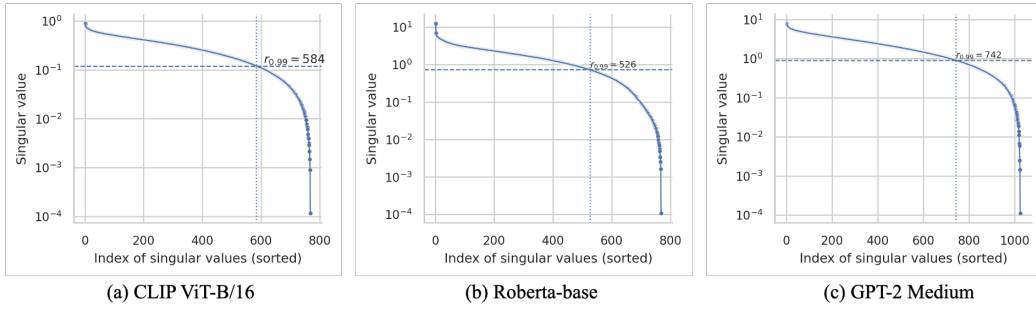


Figure 4. Spectral Decay and Effective Rank of Pre-trained Transformer Weight Matrices

C. Hyperparameter

Table 6. Hyperparameter configurations for VeFA on the E2E benchmark, for GPT-2 Medium and Large models.

| Hyperparameter | Medium | Large |
|------------------------|--------|-------|
| # GPUs | 1 | 1 |
| Optimizer | AdamW | |
| Learning Rate Schedule | Linear | |
| Weight Decay | 0.01 | |
| Batch Size | 8 | |
| Epochs | 5 | |
| Warmup Steps | 500 | |
| Label Smooth | 0.1 | |
| Learning Rate | 3E-2 | 2E-2 |

Table 5. Hyper-parameter settings for RoBERTa-Base and RoBERTa-Large on GLUE benchmark tasks.

| Model | Hyper-Parameters | SST-2 | MRPC | CoLA | QNLI | RTE | STS-B |
|-------|----------------------|--------|------|------|------|------|-------|
| Base | Optimizer | AdamW | | | | | |
| | Warmup Ratio | 0.06 | | | | | |
| | LR Schedule | Linear | | | | | |
| Base | Epochs | 60 | 30 | 80 | 25 | 80 | 50 |
| | Learning Rate (VeFA) | 1E-2 | 4E-3 | 1E-2 | 1E-2 | 4E-3 | 4E-3 |
| | Weight Decay (VeFA) | 0.05 | 0.01 | 0 | 0.01 | 0.1 | 0.1 |
| | Learning Rate (Head) | 4E-3 | 4E-3 | 1E-2 | 4E-3 | 4E-3 | 4E-3 |
| | Weight Decay (Head) | 0.05 | 0.01 | 0.01 | 0.05 | 0.1 | 0.1 |
| | Max Seq. Len. | | | 512 | | | |
| | Batch Size | | | 64 | | | |
| Large | Epochs | 40 | 20 | 20 | 25 | 20 | 20 |
| | Learning Rate (VeFA) | 1E-2 | 2E-2 | 1E-2 | 1E-2 | 2E-2 | 4E-3 |
| | Weight Decay (VeFA) | 0.1 | 0.1 | 0 | 0.01 | 0.1 | 0.1 |
| | Learning Rate (Head) | 6E-3 | 4E-3 | 4E-3 | 4E-4 | 4E-3 | 4E-3 |
| | Weight Decay (Head) | 0.1 | 0.1 | 0.01 | 0.01 | 0.1 | 0.1 |
| | Max Seq. Len. | | | 512 | | | |
| | Batch Size | | | 32 | | | |

D. Proof of Theoretical Analysis

D.1. Proof of Proposition 4.1

Since $P_{\mathcal{S}_0}^\perp$ is the projection operator admitting $P_{\mathcal{S}_0}^\perp = P_{\mathcal{S}_0}^\perp P_{\mathcal{S}_0}^{\perp T}$, the above inequality can be further written as:

$$\begin{aligned}
 \text{Tr} \left(P_{\mathcal{S}_0}^\perp \Delta \Sigma_{\mathbf{x}} \Delta^T P_{\mathcal{S}_0}^{\perp T} \right) &= \sum_i \sigma_i(\Sigma_{\mathbf{x}}) \cdot \left\| [P_{\mathcal{S}_0}^\perp \Delta Q]_{\cdot, i} \right\|_2^2 \\
 &\geq \sigma_{\min}(\Sigma_{\mathbf{x}}) \sum_i \left\| [P_{\mathcal{S}_0}^\perp \Delta Q]_{\cdot, i} \right\|_2^2 \\
 &= \sigma_{\min}(\Sigma_{\mathbf{x}}) \sum_i \left\| P_{\mathcal{S}_0}^\perp \Delta Q \right\|_F^2 \\
 &= \sigma_{\min}(\Sigma_{\mathbf{x}}) \left\| P_{\mathcal{S}_0}^\perp \Delta \right\|_F^2,
 \end{aligned}$$

in which Q is a unitary/conjugate matrix in the SVD of $\Sigma_{\mathbf{x}}$ (or equivalently orthogonal diagonalization for such symmetric matrix), and thus Q is orthogonal and is canceled in the Frobenius norm.

If we write the weight change Δ as the difference between \mathbf{W}_{ft} and \mathbf{W}_0 , the F-norm component admits:

$$\left\| P_{\mathcal{S}_0}^\perp \Delta \right\|_F \geq \left\| P_{\mathcal{S}_0}^\perp \mathbf{W}_{\text{ft}} \right\|_F - \left\| P_{\mathcal{S}_0}^\perp \mathbf{W}_0 \right\|_F.$$

in which:

$$\begin{aligned}
 P_{\mathcal{S}_0}^\perp \mathbf{W}_{\text{ft}} &= P_{\mathcal{S}_0}^\perp \sum_{i=1}^r \sigma_{\text{ft}, i} \mathbf{u}_{\text{ft}, i} \mathbf{v}_{\text{ft}, i}^T \\
 &= \sum_{i=1}^r \sigma_{\text{ft}, i} (P_{\mathcal{S}_0}^\perp \mathbf{u}_{\text{ft}, i}) \mathbf{v}_{\text{ft}, i}^T
 \end{aligned}$$

and further:

$$\begin{aligned}
 \left\| P_{\mathcal{S}_0}^\perp \mathbf{W}_{\text{ft}} \right\|_F^2 &= \text{Tr} (P_{\mathcal{S}_0}^\perp \mathbf{W}_{\text{ft}} (P_{\mathcal{S}_0}^\perp \mathbf{W}_{\text{ft}})^T) \\
 &= \sum_{i=1}^r \sigma_{\text{ft}, i}^2 \left\| P_{\mathcal{S}_0}^\perp \mathbf{u}_{\text{ft}, i} \right\|_2^2
 \end{aligned}$$

From the definition of intruder dimension above, it is straightforward that the projection of vector $\mathbf{u}_{\text{ft},i}$ onto the complement of \mathcal{S}_0 will have an upper bound $1 - \varepsilon$, and therefore:

$$\|P_{\mathcal{S}_0}^\perp \mathbf{W}_{\text{ft}}\|_F^2 > (1 - \varepsilon) \sum_{i=1}^r \sigma_{\text{ft},i}^2 \geq (1 - \varepsilon) r_{\text{ft}} \sigma_{\text{ft},r_{\text{ft}}}^2.$$

On the other hand, $\|P_{\mathcal{S}_0}^\perp \mathbf{W}_0\|_F^2 = \sum_{i=r_0+1}^r \sigma_{0,i}^2 \|P_{\mathcal{S}_0}^\perp \mathbf{u}_{0,i}\|_2^2 = \sum_{i=r_0+1}^r \sigma_{0,i}^2$ measures the residual portion of spectral power:

$$\|P_{\mathcal{S}_0}^\perp \mathbf{W}_0\|_F^2 \leq (1 - \alpha) \|\mathbf{W}_0\|_F^2.$$

Combining the two parts together, we can then derive the bound:

$$\begin{aligned} \Delta \mathcal{L} &\geq \sigma_{\min}(\Sigma_x) \|P_{\mathcal{S}_0}^\perp \Delta\|_F^2 \\ &\geq \sigma_{\min}(\Sigma_x) \left[\sqrt{(1 - \varepsilon) r_{\text{ft}} \sigma_{\text{ft},r_{\text{ft}}}^2} - \sqrt{1 - \alpha} \|\mathbf{W}_0\|_F \right]_+^2 \end{aligned}$$

D.2. Proof of Proposition 4.2

Recall that under VeFA, the fine-tuned weight matrix is $\mathbf{W}_{\text{ft}} = \mathbf{W}_0 + \mathbf{W}_0 \Lambda_k$, where $\Lambda_k = \text{diag}(\mathbf{k})$. Hence the update is $\Delta = \mathbf{W}_0 \Lambda_k$.

Since $\text{Col}(\Delta) \subseteq \text{Col}(\mathbf{W}_0) \subseteq \mathcal{S}_0$, we have $P_{\mathcal{S}_0} \Delta = \Delta$ and therefore $\text{Tr}(P_{\mathcal{S}_0} \Delta \Sigma_x \Delta^\top P_{\mathcal{S}_0}^\top) = \text{Tr}(\Delta \Sigma_x \Delta^\top)$.

We now bound this term. Because Σ_x and $\Delta \Delta^\top$ are PSD,

$$\text{Tr}(\Delta \Sigma_x \Delta^\top) = \text{Tr}(\Sigma_x \Delta^\top \Delta) \leq \|\Sigma_x\|_2 \text{Tr}(\Delta^\top \Delta) = \|\Sigma_x\|_2 \|\Delta\|_F^2.$$

Next, using sub-multiplicativity of matrix norms, we obtain

$$\|\Delta\|_F = \|\mathbf{W}_0 \Lambda_k\|_F \leq \|\mathbf{W}_0\|_F \|\Lambda_k\|_2 = \|\mathbf{W}_0\|_F \max_j |k_j|.$$

Thus

$$\|\Delta\|_F^2 \leq \|\mathbf{W}_0\|_F^2 \left(\max_j |k_j| \right)^2.$$

Combining the two bounds yields

$$\text{Tr}(P_{\mathcal{S}_0} \Delta \Sigma_x \Delta^\top P_{\mathcal{S}_0}^\top) = \text{Tr}(\Delta \Sigma_x \Delta^\top) \leq \|\Sigma_x\|_2 \|\mathbf{W}_0\|_F^2 \left(\max_j |k_j| \right)^2,$$

which is exactly the claimed inequality in Proposition 4.2.

E. Additional Numerical Experiments

E.1. Maximum VeFA Scaling Coefficient

Tables 7, 8 and 9 report the maximum VeFA scaling coefficient $\|\mathbf{k}\|_\infty$ across all layers for each task and backbone. For image classification (Table 7), all datasets yield $\|\mathbf{k}\|_\infty \leq 1.9$, indicating only mild rescaling of feature dimensions. On GLUE NLU tasks (Table 8), both RoBERTa-Base and RoBERTa-Large exhibit similarly small scaling factors, mostly in the range 1.4–3.9. For NLG with GPT-2 (Table 9), the maximal values remain below 6.2. Overall, these results confirm that VeFA operates with relatively small feature-wise scalings in practice, which is consistent with our theoretical analysis that the forgetting under VeFA is bounded and controlled by $\|\mathbf{k}\|_\infty$.

Table 7. Maximum VeFA scaling coefficient $\|\mathbf{k}\|_\infty$ on image classification tasks.

| | UCF101 | Oxford Pets | Oxford Flowers | EuroSAT | DTD | Caltech101 | Food101 |
|-------------------------|--------|-------------|----------------|---------|-------|------------|---------|
| $\ \mathbf{k}\ _\infty$ | 1.766 | 1.558 | 1.568 | 1.120 | 1.855 | 1.665 | 1.460 |

Table 8. Maximum VeFA scaling coefficient $\|k\|_\infty$ on GLUE NLU tasks.

| | CoLA | MRPC | QNLI | RTE | SST-2 | STS-B |
|---------------|-------|-------|-------|-------|-------|-------|
| RoBERTa-Base | 3.889 | 1.879 | 3.256 | 2.693 | 1.522 | 1.527 |
| RoBERTa-Large | 3.028 | 1.671 | 3.061 | 1.886 | 1.544 | 1.404 |

Table 9. Maximum VeFA scaling coefficient $\|k\|_\infty$ on NLG tasks.

| | GPT-2-Medium | GPT-2-Large |
|----------------|--------------|-------------|
| $\ k\ _\infty$ | 2.0 | 2.0 |

E.2. Average Number of Intruder Dimensions

We report the number of intruder dimensions for different GLUE tasks in Fig.5. It can be seen that LoRA consistently introduces intruder dimensions across tasks, which may exacerbate forgetting and cause conflicts when merging adapters, as shown in Tab.3. This also explains why, in our cross-task evaluations, LoRA underperforms VeFA, which by construction does not introduce any additional intruder dimensions. In particular, RTE, STS-B, and MRPC exhibit more intruder dimensions than the other three tasks, likely because they are all fine-tuned from the same MNLI checkpoint.

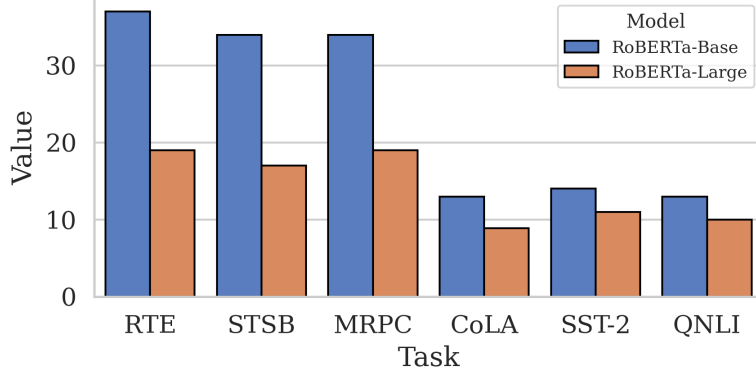


Figure 5. Number of intruder dimensions for different GLUE tasks.